Analysis of Code Phase Estimation Error From Resolved First Arrival Path

SEUNG-HYUN KONG, Member, IEEE
Korea Advanced Institute of Science and Technology
Republic of Korea

In multipath environments, a global navigation satellite system (GNSS) receiver can obtain the most correct code phase estimate from the resolved first arrival path, which is expected to have the smallest excess delay (ED). However, because of the limited performance of the code phase discriminator, multipath interference (MI), and noise, the code phase estimate can be different from that of the true first arrival path. In this paper, we derive the statistical ED distribution and power delay spectrum of GNSS multipath components based on exponential scatterer distribution model (ESDM). In parallel, we investigate the ED distributions of the first arrival path, MI, and noise to develop mathematical expressions for the code phase estimation error (CPEE) distribution for wide, narrow, and strobe correlators in various multipath channels. The mathematical models of CPEE distributions have good match with the ESDM-based CPEE distributions and the CPEE distributions obtained from Monte Carlo simulations using the International Telecommunications Union Recommendations Section recommendation P.681-7 channel model. This paper introduces one of the first theoretical analyses and models of the GNSS CPEE distributions, which can provide insights into the CPEE in multipath environments and are essential to develop algorithms against multipath distortion.

Manuscript received January 9, 2013; revised August 6, 2013, October 27, 2013; released for publication January 18, 2014.

DOI. No. 10.1109/TAES.2014.130015.

Refereeing of this contribution was handled by K. Yu.

This research was supported by a grant from Development of GNSS-Based Transportation Infrastructure Technology funded by the Ministry of Land, Transport and Maritime Affairs of the Korean government.

Author's address: Korea Advanced Institute of Science and Technology, The CCS Graduate School for Green Transportation, 291 Daehak-Ro, Yuseong-Gu, Yuseong-Gu, Daejeon 305701, Republic of Korea, E-mail: (skong@kaist.ac.kr).

I. INTRODUCTION

In multipath environments, a global navigation satellite system (GNSS) receiver may need to detect the code phase of the true first arrival path among received individual paths to obtain the most accurate code phase estimate. However, it is well known that multipath in urban environments often causes significant positioning errors, because multipath can have a large unknown excess delay (ED) relative to the line-of-sight (LOS) path [1]. In [2], an empirical power delay spectrum (PDS) obtained from massive field measurements is presented. The authors reveal that the PDS decreases exponentially with respect to ED and that the PDS decreases faster for a satellite with a higher elevation angle. The statistical ED distribution of GNSS multipath in urban environments [3] shows similar results to the observation in [2]. In addition, [2] shows that GNSS multipath has a small ED in most cases (e.g., the observed ED in the field is smaller than 0.5 μs for a satellite elevation angle above 30°) and that a stronger multipath is likely to have a smaller ED.

The effect of multipath interference (MI) on the code phase estimation is well studied in [4–6] for a two-path channel model, and MI can cause an unpredictable and large code phase estimation error (CPEE). However, the MI error, in practice, depends on the relative delay, amplitude, and phase of a number of multipath components, so the analysis of the MI error can be complicated. Because the phase of a path is uniformly random, the geometrical scatterer distribution models can be useful; they provide statistical distributions of the time of arrival (TOA) and PDS of multipath signals that related to the delay and amplitude of the multipath. In [7] and [8], mathematical expressions for TOA statistics with the Gaussian scatterer distribution model (GSDM) are introduced, and TOA statistics of multipath is analyzed experimentally in [9] and [10]. In addition to the MI, there are other causes of CPEE. The first arrival path may be a non–line-of-sight (NLOS) path with an unknown ED. Second, code phase discriminators used by receivers have limited performance in resolving the individual first arrival path. Third, noise causes a random CPEE. The preceding error causes investigated in this paper are in addition to the pseudorange errors caused by the satellite system and the atmosphere, such as errors in the satellite clock and ionospheric and tropospheric delays.

The theoretical analysis and mathematical modeling of the CPEE distribution considering NLOS propagation, MI, noise, and the code phase discriminator in various multipath channels is a complicated problem and has not been studied yet in the literature. However, thorough analysis of the CPEE is necessary to understand GNSS accuracy degradation in urban environments and to develop a GNSS positioning algorithm to cope with multipath. In this paper, we investigate the errors causing the CPEE. We also develop mathematical models of the CPEE distributions for Rician and Rayleigh channels and the code phase discriminators such as narrow, wide, and

strobe correlators. In addition, based on the exponential scatterer distribution model (ESDM), we develop the statistical ED probability density function (PDF) and PDS from which ESDM-based CPEE distributions are obtained. To show the validity of the mathematical model, the mathematical CPEE distribution models are compared to the ESDM-based CPEE distributions and the CPEE distributions obtained from numerous Monte Carlo simulations with the International Telecommunications Union Recommendations Section (ITU-R) recommendation P.681-7 model [11].

The organization of this paper is as follows. Sec. II describes the overall contribution of the ED of the true first arrival path, MI, and noise to the CPEE from the resolved first arrival path. Sec. III develops the ESDM-based ED PDF and PDS expressions, and Sec. IV focuses on the theoretical analysis of the CPEE for code phase discriminators such as wide, narrow, and strobe correlators in Rician and Rayleigh channels. Mathematical models of the CPEE distributions from the resolved first arrival path are derived in Sec. V and compared to the ESDM-based CPEE distributions and ITU-R recommendation P.681-7 land mobile satellite channel (LMSC)–based CPEE distributions in Sec. VI. Finally, Sec. VII discusses the outcome of this paper.

II. CODE PHASE ESTIMATION FROM THE RESOLVED FIRST ARRIVAL PATH

In this paper, let a short-delay path be any multipath signal arriving no later than one chip (T_c) from the LOS path [3]. In practice, there can be a set of simultaneously arriving multipath signals that build a cluster of multipath signals; therefore, short-delay paths can include multiple clusters of multipath signals with distinctive delays.

Because GNSS employs direct sequence spreading using pseudorandom noise (PRN) codes, it is easy to measure the code phase of the incoming signal simply by measuring the code phase of the distinct triangular peak from an autocorrelation function (ACF) output. An ACF output for a single path in an ideal condition contains a triangular peak at the prompt code phase of the received GNSS signal. However, in the presence of short-delay paths, an ACF output may have a peak at a code phase different from that of the true first arrival path. Alternatively, an ACF output may still have a peak at the code phase of the true first arrival path, but the code phase discriminator can return a different code phase because of the distortion of the ACF output by MI. Fig. 1 shows an example of the effect of MI on the code phase estimation with the resolved first arrival path. As shown, there are M (=7) multipath signals arriving at a GNSS receiver; their amplitudes, phases, and delays are illustrated with solid arrows. However, the receiver may be able to resolve and find only m ($= 3 \leq M$) clustered paths (i.e., m resolved paths) when the code phase discriminator cannot resolve the individual paths within each cluster. As a result, the ACF output may look like the example illustrated with

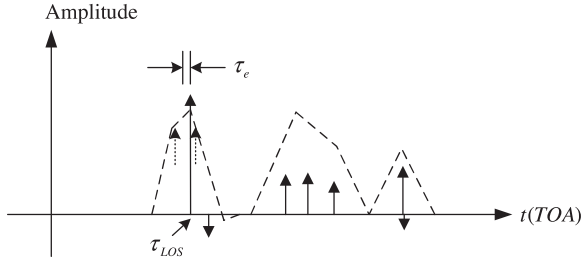

Fig. 1. Multipath and code phase estimation error from resolved first arrival path.

dash lines. Therefore, as the receiver tries to find the first arrival path, it may only find the resolved first arrival path constructed by a strong true first arrival path and a short-delay second path with a small amplitude and 180° relative phase, as shown in Fig. 1. To measure the code phase of the resolved first arrival path, the receiver employs, for example, a narrow correlator, whose early and late correlator points are depicted with two arrows using dotted lines. As illustrated, the code phase estimate using the narrow correlator [12] may yield an earlier code phase $\tau_{t_{(1)}}$ than that of the true first arrival path τ_{LOS}, resulting in a CPEE τ_e caused by the MI. In this paper, the MI error τ_e is defined as the CPEE caused by the MI

$$\tau_e = \tau_{t_{(1)}} - \tau_{T_{(1)}}, \tag{1}$$

where $\tau_{t_{(1)}}$ and $\tau_{T_{(1)}}(=\tau_{LOS})$ represent the code phases of the resolved first arrival path and the true first arrival path, respectively. As depicted in Fig. 1, the MI error depends not only on the relative amplitude, phase, and delay of the short-delay paths to the first arrival path but also on the employed code phase discriminator.

In [8], it is found that when all M ($\geq$1) multipath signal clusters are resolvable, the TOA distribution of the true first arrival path can be expressed using the first-order statistic [13] as

$$f_{T_{(1)}}(t) = M[1 - F_T(t)]^{M-1} f_T(t), \tag{2}$$

where T and $T_{(1)}$ denote the TOA and the TOA of the true first arrival path, respectively, and $F_T(t)$ and $f_T(t)$ are the TOA cumulative density function (CDF) and the TOA PDF of the GNSS multipath, respectively. The number of multipath channels M in an urban area can be about 25 $\leq M \leq$30, based on a recent report [14]. However, the exact number of paths is not a significant part of derivations in this paper. When only m ($\leq M$) paths can be resolved by the employed code phase discriminator, a GNSS receiver may try to find the code phase of the resolved first arrival path and return a TOA estimate $t_{(1)}$ that is possibly different from $T_{(1)}$. Denoting $f_{MI}(t)$ as the MI error PDF, the TOA PDF of the resolved first arrival path by the receiver when $m = 1$ can be expressed as

$$f_{t_{(1)}}(t) = f_{T_{(1)}}(t) * f_{MI}(t) \tag{3}$$

in a noiseless condition, where $*$ represents the convolution operator. In practice, noise introduces an additional CPEE, where the CPEE distribution caused by

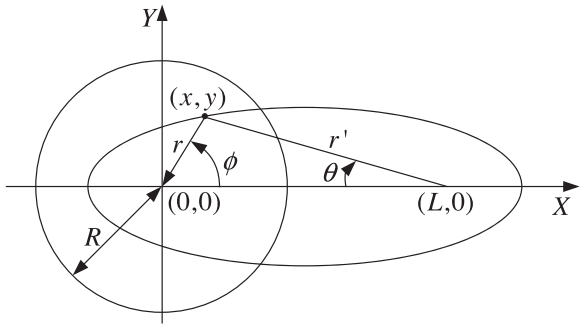

Fig. 2. Geometry of GNSS scatterer distribution.

the noise $n(t)$ is approximated by Gaussian distribution $\mathcal{N}(0, \sigma_n^2)$ [4]. Because the noise is independent from the TOA of the true first arrival path and the MI error, the overall TOA PDF of the resolved first arrival path $f_{t_{(1)}}(t)$ is expressed as

$$\begin{aligned} f_{t_{(1)}}(t) &= f_{T_{(1)}}(t) * f_{MI}(t) * f_n(t) \\ &= [M(1 - F_T(t))^{M-1} f_T(t)] * f_{MI}(t) * f_n(t) \end{aligned} \quad (4)$$

for $m = 1$. Any expression with t can be directly translated to an expression with EDτ, because τ of any individual path is related to t by $\tau = t - \tau_{LOS}$ so that the ED PDF of the resolved first arrival path can be simply found as

$$f_{\tau_{(1)}}(\tau) = f_{t_{(1)}}(t)|_{t=\tau+\tau_{LOS}}. \quad (5)$$

In this paper, we consider $m = 1$ as one of the most common cases for a receiver in urban environments, where visible satellites are likely to be at high elevation angles and the maximum ED is less than 1 chip in general [2]. In practice, there can be numerous multipath signals arriving at a receiver in urban environments, but only a small number of them are dominant paths. It is assumed that those dominant multipath signals occur independently, so their amplitudes, phases, and delays are also independent. Because the MI error depends on the relative code phase, amplitude, and phase of short-delay paths to those of the true first arrival path and on the code phase discriminator in the receiver, we assume that the ED of the true first arrival path and the MI error are statistically independent. In Secs. IV and V, mathematical expressions for (4) in Rician and Rayleigh channels are derived.

III. ESDM-BASED TOA PDF AND PDS

In parallel with deriving a mathematical model for the CPEE distribution, we develop the statistical TOA PDF and PDS based on a geometrically based single bounce circular model that is often used to obtain a statistical channel model when the transmitter is above the receiver and the scattering objects [15]. Then, the TOA PDF and PDS can be used to generate statistical multipath channels from which ACF outputs are obtained, and various code phase discriminators are applied to the ACF outputs to find statistical CPEE distributions.

Fig. 2 illustrates a geometry, shown on the horizontal plane, to derive the TOA PDF and PDS of the GNSS multipath in urban environments. A GNSS receiver is located at the origin of an xy-coordinate system and a polar (r, ϕ) coordinate system, where $\phi = 0$ aligns with the positive x-axis. A scatterer and a GNSS satellite are located at (x, y) and $(L, 0)$ in the xy-coordinate system, respectively, or, equivalently, at (r, ϕ) and $(L, 0)$ in the polar coordinate system, respectively. The radius R of the circular region represents a distance that the existence of scatterers causing a multipath to the receiver becomes negligibly small.

The shape, size, and scatterer density distribution are still subject to debate [15], but the statistical observation in [2, 3, 7, 8] and [14] is that scatterers farther away (larger r) are less likely to produce multipath to the receiver. There have been various scatterer distribution models introduced in the literature, for example, uniform [16] and [17], Gaussian [7] and [8], and exponential [18] scatterer distribution models, and the TOA PDF and PDS based on them exhibit similarities to the field observations. However, for the uniform scatterer distribution model (USDM) and GSDM, there are numerous point locations around a GNSS receiver where the probability for every point location to have a scatterer generating a multipath to the receiver is the same as or similar to the probability to have an LOS path because the scatterer density at every point location around and at the receiver is the same or similar. The field observation in [2] and [14] shows that the largest scatterer density is at the receiver (causing the LOS path) and that the density of scatterers decreases gradually with respect to r over a wide area, which shows that the ESDM can be a more suitable model than the USDM and GSDM, as observed in [18]. Therefore, in this paper, we use the ESDM to derive expressions for the statistical TOA PDF and PDS derivation, which can be expressed as

$$f_{x,y}(x, y) = \begin{cases} \dfrac{C_0}{2\pi r_o^2} \exp\left(-\dfrac{\sqrt{x^2 + y^2}}{r_o}\right), & \sqrt{x^2 + y^2} \le R \\ 0, & \text{otherwise,} \end{cases} \quad (6)$$

where C_0 is a constant that normalizes the $f_{x,y}(x, y)$. Analogous to the σ used in the two-dimensional (2D) GSDM [7] and [8], r_o represents the spread of scatterers and is related to the satellite elevation such that $r_o = r_c \cos(E)$ [3], where r_c represents the spread of scatterers in the horizontal plane and E is the satellite elevation angle.

In Fig. 2, scatterer locations causing the same ED τ are depicted by an ellipse, provided that the satellite and the receiver are located at the foci of the ellipse. A NLOS path with an azimuth of departure θ is reflected from a scatterer at (x, y) and arrives at the receiver with an azimuth of arrival (AOA) ϕ after propagating TOA $t = (r + r')/c$ s, where r' is the distance from the satellite to the scatterer. Because $x = r\cos(\phi)$ and $y = r\sin(\phi)$, the radial distribution of scatterers can be expressed in terms of r as

$$f_r(r) = \frac{r}{r_o^2} \exp\left(-\frac{r}{r_o}\right), \quad \text{for } r \ge 0. \quad (7)$$

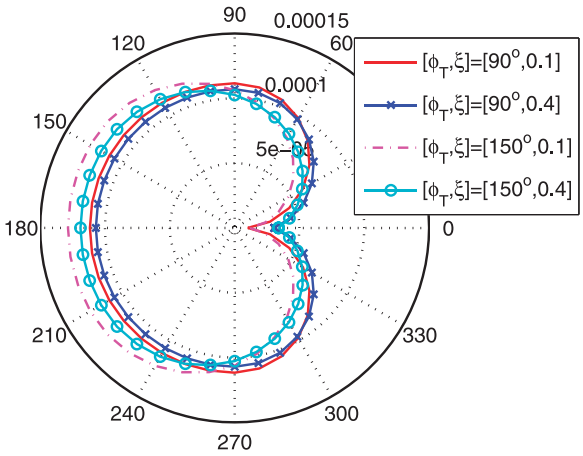

Fig. 3. $f_{r,\phi|E}(r,\phi|E)$ with $r = r_o = 100$ m.

In [2] and [3], it is found that ϕ is not uniformly distributed, and exploiting the AOA PDF $f_\phi(\phi)$ in [3], $f_{x,y}(x, y)$ (6) can be expressed in terms of (r, ϕ) as

$$f_{r,\phi|E}(r,\phi|E) = \begin{cases} \dfrac{kr}{4\pi^2 r_o^2}\exp\left(-\dfrac{r}{r_o}\right), \\ \qquad \text{for } r \le R \text{ and } \phi_T < |\phi| \le \pi \\ \dfrac{kr[\xi+\sin(\alpha|\phi|)]}{4\pi^2(1+\xi)r_o^2}\exp\left(-\dfrac{r}{r_o}\right), \\ \qquad \text{for } r \le R \text{ and } |\phi| \le \phi_T \\ 0, \quad \text{otherwise}, \end{cases} \tag{8}$$

where $\phi_T (0 \ll \phi_T \le \pi)$ is an environment-dependent AOA above which the most multipath signals are arriving at the receiver [3], $\alpha = \frac{\pi}{2\phi_T}$, ξ $(0 \le \xi < 1)$ decides the density at $\phi = 0$, and k is a constant that normalizes $f_\phi(\phi)$ as

$$k = \frac{\pi\alpha(1+\xi)}{\alpha(\pi - \phi_T + \pi\xi) + 1}. \tag{9}$$

Fig. 3 shows an example of $f_{r,\phi|E}(r, \phi|E)$ for some ϕ_T and ξ, when $r = r_o = 100$ m and a GNSS satellite is at $\phi = 0$ and $E = 0$. The shape of the plots in Fig. 3 shows the marginal AOA PDF $f_\phi(\phi)$ [3] and is similar to the empirical AOA PDF [14] in that the largest density is at $\phi = \pi$ and the density decreases as the ϕ decreases in general. In addition, $\phi_T = 150^\circ$ results in a better match with the empirical AOA PDF [14] than $\phi_T = 90^\circ$. However, the major difference is that $f_\phi(\phi)$ in Fig. 3 has a larger density than the empirical AOA PDF for $|\phi| \le \phi_T$ and any ϕ_T and ξ [14]. Therefore, in the following analysis, we assume that $f_\phi(\phi)$ has a smaller density for $|\phi| \le \phi_T$ in practice than does the algebraic model [3] used in (8).

The PDS $f_P(t)$ of the GNSS multipath describes the likelihood distribution of the received GNSS signal power with respect to the TOA t. Because $r' \simeq L \gg r$ (e.g., $r \ll 10$ km and $L \ge 20\,200$ km in global positioning system) in Fig. 2, the signal attenuation because of the propagation from the satellite to the scatterers near the GNSS receiver is similar so that the signal power arriving at any scatterer represented by any elemental area $dxdy$ is statistically the same for all scatterers [7]. In addition, the expected signal power scattered to the receiver is statistically the same for all scatterers. Therefore, the received signal power of a NLOS path scattered from a scatterer at distance r can be expressed as $P(r) = C_1 r^{-\gamma}$ [7], where C_1 represents the signal power scattered to the receiver from a scatterer and $\gamma \simeq 2$ is the free space attenuation exponent. Denoting τ as the ED of multipath,

$$\tau c = tc - L \simeq \frac{r[1-\cos(\phi)]}{\cos(E)} \tag{10}$$

from [3]. If, for a moment, we assume $f_\phi(\phi) = 1/(2\pi)$, then the PDF of the ED τ (10) can be found using the relationship $f_{\tau|r}(\tau|r) = (\partial\phi/\partial\tau) f_\phi(\phi)$ as

$$f_{\tau|r}(\tau|r) = \begin{cases} \dfrac{c\sqrt{\cos(E)}}{\pi\sqrt{\tau c[2r - \tau c\cos(E)]}}, & 0 < \tau c < \dfrac{2r}{\cos(E)} \\ 0, & \text{otherwise}. \end{cases} \tag{11}$$

Exploiting the field observation in [14], $f_{r,\phi|E}(r, \phi|E)$ in (8) has the most density within $\phi_T \le |\phi| \le \pi$, so the scatterer density for $|\phi| < \phi_T$ can be neglected and

$$\frac{r[1-\cos(\phi_T)]}{\cos(E)} \le \tau c \le \frac{2r}{\cos(E)}. \tag{12}$$

When ϕ_T is large (e.g., $\phi_T \ge 150^\circ$), the expression in (12) can be approximated as

$$\tau c \simeq \frac{2r}{\cos(E)}. \tag{13}$$

Because the probability of having a scatterer at radius r is $f_r(r)$ (7), the PDS $f_P(\tau)$ can be approximated using (13) as

$$\begin{aligned} f_P(\tau) &\simeq C_2' \left|\frac{\partial r}{\partial \tau}\right| P(r) f_r(r)|_{r=\frac{\tau c}{2}\cos(E)} \\ &\simeq C_2 \tau^{1-\gamma} \exp\left(-\frac{\tau}{\tau_o}\right) \end{aligned} \tag{14}$$

where $\tau_o = 2r_o/[c\cos(E)]$ and

$$C_2 = \left[\log\frac{2R}{c\delta_\tau\cos(E)} + \sum_{k=1}^{\infty}\frac{(-1)^k}{k\cdot k!\tau_o^k}\left[\left(\frac{2R}{c\cos(E)}\right)^k - \delta_\tau^k\right]\right]^{-1} \tag{15}$$

for $\gamma = 2$. Because it is the PDS of the multipath, $f_P(\tau)$ (14) is only defined for $\tau > 0$. Similarly, the ED PDF $f_\tau(\tau)$ for $\tau > 0$ is found as

$$\begin{aligned} f_\tau(\tau) &\simeq \left|\frac{\partial r}{\partial \tau}\right| f_r(r)|_{r=\frac{\tau c}{2}\cos(E)} \\ &\simeq \frac{\tau}{\tau_o^2}\exp\left(-\frac{\tau}{\tau_o}\right). \end{aligned} \tag{16}$$

IV. MATHEMATICAL MODELING OF MI ERROR DISTRIBUTION

In Sec. II, we defined the MI error (i.e., the CPEE because of the MI) as occurring when ACF output is

distorted by short-delay paths. Strictly speaking, causes other than multipath contribute to the MI error. For example, the finite bandwidth of the GNSS signals, the narrow bandpass filter [4], and the code phase discriminator employed by a receiver contribute to the limited resolution in distinguishing the true first arrival path among the short-delay paths. In the following analysis, we assume that an ACF output for a single path has an ideal sharp triangular peak. Therefore, to derive the MI error PDF $f_{MI}(t)$, we focus on the performance analysis of code phase discriminators in the presence of short-delay paths. In this section and in the following analysis, we consider Rician and Rayleigh channels for general multipath channels in practice.

A. Rician Channel

In general, a channel impulse response in multipath environments is expressed as

$$h_1(t) = \sum_{n=1}^{N} a_n e^{-j\theta_n} \delta(t - \tau_{(n)}), \tag{17}$$

where a_n, $\tau(n)$, and θ_n are the magnitude, ED, and phase of the nth arrival path, respectively. In addition, a_n (for $n \geq 2$) follows the Rayleigh distribution [13], and the likelihood distributions of a_n^2, τ, and θ_n (for $n \geq 2$) are $f_P(\tau)$ (14), $f_\tau(\tau)$ (16), and uniform distribution in $[0, 2\pi)$ [16] and [19], respectively. This means that a path with a smaller delay is likely to occur more often and is likely to have a higher power. In a Rician channel, the first arrival path is the LOS path, so the distribution of the first arrival path is

$$\begin{aligned} f_{\tau_{(1)}}(\tau) &= f_{T_{(1)}}(t)|_{t=\tau+\tau_{LOS}} \\ &= \delta(t - \tau_{LOS}), \end{aligned} \tag{18}$$

and the power ratio of the LOS path to all multipath components is denoted by

$$K = \frac{a_1^2}{\sum_{n=2}^{N} E\left[a_n^2\right]} \gg 1. \tag{19}$$

In this subsection, short-delay paths ($2 \leq n \leq N$) in (17) are modeled by a single path exploiting the analysis in [3]. The following two-path channel model may be vulnerable for a low-elevation-angle satellite channel, in which multiple resolved paths can be observed. When the receiver has phase lock on the strongest path that dominates the resolved path, all signal components appear in the in-phase arm [3] and the expression for $h_1(t)$ can be simplified to

$$h_1(t) \simeq \alpha_1 \delta(t - \tau_{LOS}) + \alpha_t \delta(t - \tau_t), \tag{20}$$

where

$$\alpha_1 \simeq a_1, \tag{21a}$$

$$\alpha_t \simeq \sum_{n=2}^{N} a_n \cos \psi_n, \tag{21b}$$

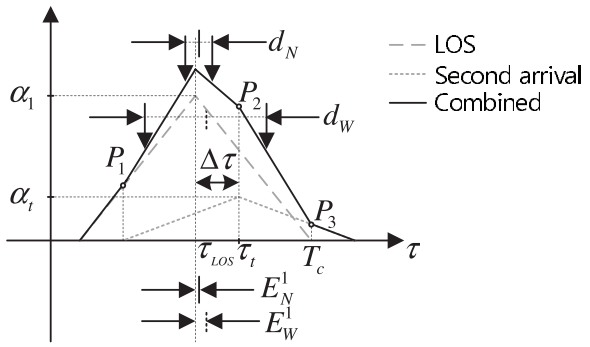

Fig. 4. ACF output in urban multipath channel environments.

$$\psi_n \approx \theta_n - \theta_1, \tag{21c}$$

$$\tau_{(2)} \leq \tau_t \leq \tau_{(N)}, \tag{21d}$$

and the net amplitude α_t follows the Gaussian distribution [19]. Fig. 4 illustrates an example of an ACF output $g_o(\tau)$ for a two-path Rician channel, where the first path (of the two) is the LOS path and the second path is a weak short-delay path that is constructed by a sum of closely spaced short-delay paths. When τ is the code phase difference between the received signal and a receiver-generated code replica, a normalized ACF output for a single path channel can be expressed as

$$R(\tau) = \begin{cases} 1 - |\tau|/T_c + n(\tau), & |\tau| < T_c \\ n(\tau) + p(\tau), & \text{otherwise,} \end{cases} \tag{22}$$

where $n(\tau)$ and $p(\tau)$ represent the sum of noise samples and cross-correlation between the GNSS PRN codes, respectively. Therefore, the ACF output in Fig. 4 can be expressed as

$$g_o(\tau) = h_1(t)|_{t=\tau+\tau_{LOS}} * R(\tau), \tag{23}$$

where $*$ represents the convolution operator. In the following analysis, we neglect $p(\tau)$, because $|p(\tau)| \ll 1$ [4]. Let $\tau_{(1)} = \tau_{LOS} = 0$, P_1, P_2, and P_3 in Fig. 4 be the points at $(\tau_t - T_c, \alpha_1\tau_t/T_c)$, $(\tau_t, \alpha_1 + \alpha_t - \alpha_1\tau_t/T_c)$, and $(T_c, \alpha_t\tau_t/T_c)$, respectively. To see the effect of code phase discriminators on the MI error, we apply wide, narrow, and strobe correlators [12] to $g_o(\tau)$. In general, wide and narrow correlators use a set of early and late correlators with correlator spacing d equal to d_W ($= 1.0T_c$) and d_N ($= 0.1T_c$ usually), respectively, and strobe correlator uses two sets of early and late correlators with $d = 0.1T_c$ and $d = 0.2T_c$, for example. Because $K \gg 1$, $\alpha_1 \gg \alpha_t$, and the MI error ε_1 can be found as

$$\varepsilon_1 \simeq \begin{cases} \dfrac{\Delta\tau\alpha_t}{\alpha_1}, & \tau_t \leq \tau_L \\ \dfrac{d\alpha_t}{2\alpha_1}, & \tau_L < \tau_t \leq T_c + \tau_E \\ (T_c + \dfrac{d}{2} - \Delta\tau)\dfrac{\alpha_t}{\alpha_1}, & \tau_E + T_c < \tau_t \leq T_c + \tau_{LOS} + \dfrac{d}{2} \\ 0, & \text{otherwise,} \end{cases} \tag{24}$$

after some algebraic manipulations exploiting [3], where $(\cdot)_1$ denotes the Rician channel; τ_E and τ_L are the code phases of the early and late correlators, respectively; $d = \tau_L - \tau_E$; and $\Delta\tau = \tau_t - \tau_{LOS} \le d/2$. The MI error (24) is independent from the ED of the first path τ_{LOS} but depends on the amplitude ratio α_t/α_1, relative delay $\Delta\tau$, and correlator spacing d. The statistical values of α_t/α_1 and $\Delta\tau$ are obtainable from the ED PDF $f_\tau(\tau)$ and PDS $f_P(\tau)$, and d depends on the employed code phase discriminator. In addition, for a narrow correlator, $\tau_L \approx \tau_{LOS} + 0.05T_c$ and $\tau_E \approx \tau_{LOS} - 0.05T_c$, and for a wide correlator, $\tau_L \approx \tau_{LOS} + 0.5T_c$ and $\tau_E \approx \tau_{LOS} - 0.5T_c$ when α_t/α_1 is small ($\ll$1). Because $\tau_t \le \tau_{(N)} \le 0.5T_c$, it is expected that the narrow correlator observes $\tau_t \le \tau_L$ or $\tau_t > \tau_L$ and the wide correlator experiences $\tau_t \le \tau_L$ in most cases. Therefore, the MI error (24) for the narrow and wide correlators can be expressed as

$$\varepsilon_{1,N} \le \frac{d_N \alpha_t}{2\alpha_1} \tag{25}$$

and

$$\varepsilon_{1,W} \simeq \frac{\Delta\tau \alpha_t}{\alpha_1}, \tag{26}$$

respectively, where the inequality in (25) is to include the case when $\Delta\tau < d_N/2$. Because α_1 is the amplitude of the LOS path, the variation of α_1 is negligibly small comparing to α_t, which has a normal distribution for $N \gg 2$ [19]. Therefore, when the receiver has phase lock to the strongest path (i.e., the LOS path), α_1 can be assumed constant in the baseband, and the distribution of $u_1 = \alpha_t/\alpha_1$ is

$$f_{u_1}(u) \simeq f_{u_1}^{\mathcal{N}}\left(u; 0, \sigma_{u_1}^2\right), \tag{27}$$

where $\sigma_{u_1}^2$ is the variance of u_1 so that the variance of $\varepsilon_{1,N}$ (25) and $\varepsilon_{1,W}$ (26) are

$$\sigma_{1,N}^2 = \mathrm{Var}[\varepsilon_{1,N}] \le \frac{d_N^2}{4}\sigma_{u_1}^2 \tag{28}$$

and

$$\sigma_{1,W}^2 = \mathrm{Var}[\varepsilon_{1,W}] \simeq \Delta\tau^2 \sigma_{u_1}^2, \tag{29}$$

respectively. Because $0 \le \Delta\tau \le 0.5T_c$ for a satellite elevation angle above 30°, $\Delta\tau$ can be larger than $d_N/2 = 0.05T_c$, often so that $\sigma_{1,W} > \sigma_{1,N}$ is expected in general. In summary, the PDFs of $\varepsilon_{1,N}$ (25) and $\varepsilon_{1,W}$ (26) are

$$f_{MI_{1,N}}(\tau) \simeq f_\tau^{\mathcal{N}}\left(\tau; 0, \sigma_{1,N}^2\right) \tag{30}$$

and

$$f_{MI_{1,W}}(\tau) = f_\tau^{\mathcal{N}}\left(\tau; 0, \sigma_{1,W}^2\right), \tag{31}$$

respectively, where $f_\tau^{\mathcal{N}}(\tau; \mu, \sigma^2)$ represents the normal distribution of ED τ with mean μ and variance σ^2 and $(\cdot)_N$ and $(\cdot)_W$ denote the narrow and wide correlators, respectively. The MI error for a strobe correlator is similar to that for the narrow correlator if τ_t is very small or around T_c, but it is zero otherwise [12]. Therefore, the MI error for a strobe correlator in the Rician channel is

$$f_{MI_{1,S}}(\tau) \simeq \begin{cases} f_\tau^{\mathcal{N}}\left(\tau; 0, \sigma_{1,S}^2\right), & \text{for } \tau \approx 0 \text{ or } T_c \\ \delta(\tau), & \text{otherwise,} \end{cases} \tag{32}$$

where $(\cdot)_S$ denotes the strobe correlator and $\sigma_{1,S} = \sigma_{1,N}$. Because $f_{\tau_{(1)}}(\tau) = \delta(\tau)$ from (18), the MI error PDF for the narrow, wide, and strobe correlators in the noiseless Rician channel are

$$f_{\varepsilon_{1,N}}(\tau) \simeq f_{\tau_{(1)}}(\tau) * f_\tau^{\mathcal{N}}\left(\tau; 0, \sigma_{1,N}^2\right) = f_\tau^{\mathcal{N}}\left(\tau; 0, \sigma_{1,N}^2\right), \tag{33}$$

$$f_{\varepsilon_{1,W}}(\tau) \simeq f_{\tau_{(1)}}(\tau) * f_\tau^{\mathcal{N}}\left(\tau; 0, \sigma_{1,W}^2\right) = f_\tau^{\mathcal{N}}\left(\tau; 0, \sigma_{1,W}^2\right), \tag{34}$$

and

$$f_{\varepsilon_{1,S}}(\tau) = f_{\tau_{(1)}}(\tau) * f_{MI_{1,S}}(\tau) = f_{MI_{1,S}}(\tau), \tag{35}$$

respectively.

B. Rayleigh Channel

When the LOS path is severely attenuated or blocked, a number of short-delay paths arriving at a GNSS receiver dominate and constitute the resolved first arrival path. Considering the ED PDF $f_\tau(\tau)$ (16) and the ED PDS $f_P(\tau)$ (14), a short-delay path with a smaller ED is likely to occur more often and to have a higher signal power. However, the power difference between the true first arrival path and a short-delay path is not as large as that in the Rician channel. In this subsection, we derive the MI error PDF in Rayleigh channels using the two-path channel model [3], where each path maybe constructed by a group of closely arriving N_1 ($1 \le N_1 \le M - N_2$) and N_2 ($1 \le N_2 \le M - N_1$) paths, respectively.

Fig. 4 also illustrates an ACF output in a Rayleigh channel; the first path and the second path have peaks at nonzero EDs $\tau_{(1)}$ ($>\tau_{LOS}$) and τ_t ($>\tau_{(1)}$) with amplitudes α_1 and α_t ($|\alpha_1| \ge |\alpha_t|$), respectively. Here, $|\alpha_1| \ge |\alpha_t|$ and $|\alpha_1| < |\alpha_t|$ are equally likely to occur when $\tau_t - \tau_{(1)}$ is very small, but $|\alpha_1| \ge |\alpha_t|$ is more likely to be observed as $\tau_t - \tau_{(1)}$ increases, because the second path is a sum of short-delay paths with small amplitudes that are exponentially decreasing with $\tau_t - \tau_{(1)}$. However, when $\tau_t - \tau_{(1)}$ is small, the two path may be viewed as a single path. Therefore, $|\alpha_1| \ge |\alpha_t|$ is assumed as a dominant case in Rayleigh channels.

Because the GNSS receiver successfully tracks the phase of the strongest path, the phase of the first path (of the two) becomes negligibly small so that $|\alpha_1| = \alpha_1 > 0$, and the impulse response in Rayleigh channels can be expressed as

$$h_2(t) \simeq \alpha_1 \delta(t - \tau_{(1)}) + \alpha_t \delta(t - \tau_t), \tag{36}$$

where

$$\alpha_1 \simeq \sum_{n_1=1}^{N_1} a_{n_1} \cos(\theta_{n_1} - \psi_1) \tag{37a}$$

$$\alpha_t \simeq \sum_{n_2=N_1+1}^{N} a_{n_2} \cos(\theta_{n_2} - \psi_1) \tag{37b}$$

$$\psi_1 = \arg\min_{\psi} \left| \alpha_1 e^{-j\psi} - \sum_{n_1=1}^{N_1} a_{n_1} e^{-j\theta_{n_1}} \right|^2 \tag{37c}$$

$$\tau_{(1)} \le \tau_1 \le \tau_{(N_1)} \tag{37d}$$

$$\tau_{(N_1+1)} \le \tau_t \le \tau_{(N_2)}. \tag{37e}$$

Both amplitudes α_1 and α_t follow the Gaussian distribution [19], and $|\alpha_1| > |\alpha_t|$ is assumed. Using (25) and (26), the MI errors for narrow and wide correlators are expressed as the sum of the ED of the first path $\tau_{(1)}$ and the MI error as

$$\varepsilon_{2,N} \le \tau_{(1)} + \frac{d_N \alpha_t}{2\alpha_1} \tag{38}$$

and

$$\varepsilon_{2,W} \simeq \tau_{(1)} + \frac{\Delta\tau \alpha_t}{\alpha_1} \tag{39}$$

respectively, where $(\cdot)_2$ denotes the Rayleigh channel. Exploiting (32), the MI error of a strobe correlator can be expressed as

$$\varepsilon_{2,S} \le \begin{cases} \tau_{(1)} + \dfrac{d_N \alpha_t}{2\alpha_1}, & \tau_t \simeq \tau_{(1)} \text{ or } \tau_{(1)}+T_c \\ \tau_{(1)}, & \text{otherwise,} \end{cases} \tag{40}$$

where $(\cdot)_S$ denotes the strobe correlator. When $u_2 = \alpha_t/\alpha_1$, it is found that u_2 ($|u_2| < 1$) has a truncated Cauchy distribution with zero mean and variance $\sigma_{u_2}^2 (> \sigma_{u_1}^2)$:

$$\sigma_{u_2}^2 = \frac{2\sigma_t}{\pi\sigma_f}\left[1 - \frac{\sigma_t}{\sigma_f}\tan^{-1}\left(\frac{\sigma_f}{\sigma_t}\right)\right], \tag{41}$$

where σ_f and σ_t represent the standard deviations of α_1 and α_t, respectively. Because α_1 and α_t depend on the multipath situation in the surrounding environments, σ_f and σ_t can vary when an environment changes. Therefore, the statistical distribution of u_2 is a sum of Cauchy distributions with different values of σ_f and σ_t, which can be approximated by a normal distribution as

$$f_{u_2}(u) \simeq f_{u_2}^{\mathcal{N}}(u; 0, \sigma_{u_2}^2). \tag{42}$$

Like the variances in the Rician channel (28) and (29), the variances of the MI error for narrow, wide, and strobe correlators are found as

$$\sigma_{2,N}^2 = \mathrm{Var}[\varepsilon_{2,N} - \tau_{(1)}] \le \frac{d_N^2}{4}\sigma_{u_2}^2, \tag{43}$$

$$\sigma_{2,W}^2 = \mathrm{Var}[\varepsilon_{2,W} - \tau_{(1)}] \simeq \Delta\tau^2 \sigma_{u_2}^2, \tag{44}$$

and

$$\sigma_{2,S}^2 \le \sigma_{2,N}^2, \tag{45}$$

respectively. The equality in (43) holds for $\Delta\tau \le d_N/2$ [12]. Using (43)–(45), the approximate MI error distributions for narrow and wide correlators in the Rayleigh channel are expressed as

$$f_{MI_{2,N}}(\tau) \simeq f_\tau^{\mathcal{N}}(\tau; 0, \sigma_{2,N}^2) \tag{46}$$

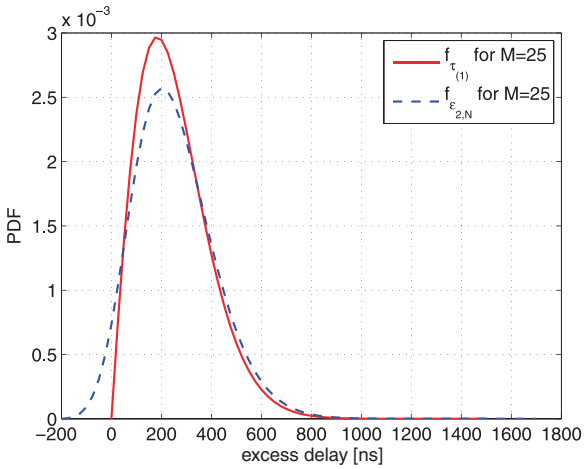

Fig. 5. CPEE distribution in Rayleigh channel.

and

$$f_{MI_{2,W}}(\tau) \simeq f_\tau^{\mathcal{N}}(\tau; 0, \sigma_{2,W}^2), \tag{47}$$

respectively, and that for the strobe correlator is found as

$$f_{MI_{2,S}}(\tau) \simeq \begin{cases} f_\tau^{\mathcal{N}}(\tau; 0, \sigma_{2,N}^2), & \text{for } \Delta\tau \le \dfrac{d_N}{2} \text{ or } T_c \\ \delta(\tau), & \text{otherwise,} \end{cases} \tag{48}$$

where $\sigma_{2,S} = \sigma_{2,N}$.

Letting M be the number of individual paths arrived at the receiver with detectable power (i.e., nonnegligible power), the ED PDF of the first arrival path is expressed using the order statistic [13] and exploiting (2) as

$$\begin{aligned} f_{\tau_{(1)}|(M,\tau_o)}(\tau) &= M[1 - F_\tau(\tau)]^{M-1} f_\tau(\tau) \\ &= \frac{M\tau(\tau+\tau_o)^{M-1}}{\tau_o^{M+1}} \exp\left(-\frac{M\tau}{\tau_o}\right), \end{aligned} \tag{49}$$

where the ED CDF $F_\tau(\tau)$ is obtained from (16) as

$$F_\tau(\tau) = 1 - \left(1 + \frac{\tau}{\tau_o}\right)\exp\left(-\frac{\tau}{\tau_o}\right) \tag{50}$$

and τ_o is defined in (14). The statistical mean of $\tau_{(1)}$ increases with τ_o as the distribution $f_{t_{(1)}|(M,\tau_o)}(\tau)$ becomes wider, and it decreases as M increases. Integrating the expressions in (46)–(48) with (49), the CPEE distributions in a noiseless Rayleigh channel are found as

$$f_{\varepsilon_{2,N}}(\tau) \simeq f_{\tau_{(1)}|(M,\tau_o)}(\tau) * f_\tau^{\mathcal{N}}(\tau; 0, \sigma_{2,N}^2), \tag{51}$$

$$f_{\varepsilon_{2,W}}(\tau) \simeq f_{\tau_{(1)}|(M,\tau_o)}(\tau) * f_\tau^{\mathcal{N}}(\tau; 0, \sigma_{2,W}^2), \tag{52}$$

and

$$f_{\varepsilon_{2,S}}(\tau) = f_{\tau_{(1)}|(M,\tau_o)}(\tau) * f_{MI_{2,S}}(\tau) \tag{53}$$

for narrow, wide, and strobe correlators, respectively. Fig. 5 shows the numerical evaluation of $f_{\tau_{(1)}|(M,\tau_o)}(\tau)$ and $f_{\varepsilon_{2,N}}(\tau)$ for $M = 25$, $\tau_o = 1$ μs, and $\sigma_{2,N} = 0.08$ μs.

The preceding expressions (51)–(53) are all based on the statistical assumption $|\alpha_1| > |\alpha_t|$. When $|\alpha_1| < |\alpha_t|$, the receiver has a phase lock to the second path so that

$|\alpha_1| < \alpha_t$. The means of $\varepsilon_{2,N}$ (38), $\varepsilon_{2,W}$ (39), and $\varepsilon_{2,S}$ (40) become the same to τ_t, and the second terms in (38)–(40) become opposite so that

$$\varepsilon'_{2,N} \le \tau_t \frac{d_N \alpha_1}{2\alpha_t}, \tag{54}$$

$$\varepsilon'_{2,W} \simeq \tau_t \frac{\Delta\tau \alpha_1}{\alpha_t}, \tag{55}$$

and

$$\varepsilon'_{2,S} \le \tau_t \frac{d_N \alpha_1}{2\alpha_t}, \tag{56}$$

respectively, for $\tau_t \simeq \tau_{(1)}$ or $\tau_{(1)} + T_c$. Therefore, we can expect that $\varepsilon'_{2,N}$, $\varepsilon'_{2,W}$, and $\varepsilon'_{2,S}$ have larger means (i.e., $\tau_t > \tau_{(1)}$) and different variances from $\varepsilon_{2,N}$, $\varepsilon_{2,W}$, and $\varepsilon_{2,S}$, respectively, because (49) should be modified for the N_tth arrival path ($N_1 < N_t \le N_2$).

V. OVERALL CPEE DISTRIBUTIONS

In addition to the ED of the first arrival path and the MI error, final code phase estimation accuracy is degraded by the noise $n(\tau)$ in the ACF output. In this section, we derive mathematical expressions for the overall CPEE from the resolved first arrival path.

A. Rician Channel

Because the CPEEs resulting from the noise and the MI error are mutually independent, final code phase estimated from the resolved first arrival path in a Rician channel has an ED τ distributed as

$$\begin{aligned} f_{\tau,1}(\tau) &= f_{MI_1}(\tau) * f_{n,1}(\tau) \\ &\approx f_\tau^{\mathcal{N}}(\tau; 0, \sigma_1^2), \end{aligned} \tag{57}$$

where $f_{MI,1}(\tau)$ is defined in (30), (31) or (32) and $f_{n,1}(\tau)$ is the distribution of the CPEE because of the noise $n(\tau)$ (22) in the ACF output. In the following analysis, additive white Gaussian noise is assumed in the signal samples, and the effect of noise on the CPEE is approximated by a normal distribution $f_n(\tau)$, as in [4].

Let A be the peak amplitude of an ACF output, i.e., $h_1(\tau) * R(\tau)$; δ_τ be the CPEE because of the noise; and N_E and N_L represent the noise amplitudes at the early and late correlator outputs, respectively. Then, in [4],

$$\delta\tau \simeq \frac{T_c(N_E - N_L)}{2A}, \tag{58}$$

and the variance of δ_τ is

$$\sigma^2_{\delta\tau}(d) = \begin{cases} \dfrac{T_c^2 d_N N_0}{4A^2 T}, & \text{for the narrow correlator : } d = d_N \\ \dfrac{T_c^2 d_W N_0}{4A^2 T}, & \text{for the wide correlator : } d = d_W, \end{cases} \tag{59}$$

where T is the correlation length and $d = d_N$ and $d = d_W$ are used for the narrow and wide correlators, respectively. Because $d_N = 0.1T_c$ and $d_W = 1T_c$ is a common choice, the narrow correlator has $\beta = d_W/d_N = 10$ times smaller variance of the CPEE than the wide correlator.

Let d_1 and d_2 be the correlator spacings (usually, $d_1 = 0.1T_c$ and $d_2 = 0.2T_c$) used for a strobe correlator. Then, the discriminator function can be expressed as [12]

$$\begin{aligned} L_\tau = {} & 2(S_{E,1} - S_{L,1}) - (S_{E,2} - S_{L,2}) \\ & + 2(N_{E,1} - N_{L,1}) - (N_{E,2} - N_{L,2}), \end{aligned} \tag{60}$$

where $S_{E,1} = AR(\delta_\tau - d_1/2)$, $S_{E,2} = AR(\delta_\tau - d_2/2)$, $S_{L,1} = AR(\delta_\tau + d_1/2)$, and $S_{L,2} = AR(\delta_\tau + d_2/2)$ represent the signal components and $N_{E,1}$, $N_{E,2}$, $N_{L,1}$, and $N_{L,2}$ represent the noise components $n(\tau)$ contained in the ACF output samples at four consecutive code phases $\delta_\tau - d_1/2$, $\delta_\tau - d_2/2$, $\delta_\tau + d_1/2$, and $\delta_\tau + d_2/2$, respectively. Exploiting the analysis in [4], it can be found that

$$\delta\tau_S = \frac{2T_c(N_{E,1} - N_{L,1})}{4A} - \frac{T_c(N_{E,2} - N_{L,2})}{2A} \tag{61}$$

and that

$$\begin{aligned} \sigma^2_{\delta\tau_S} &= \frac{T_c^2}{4A^2}\mathrm{Var}\{N_{E,1} - N_{L,1} - N_{E,2} + N_{L,2}\} \\ &= \frac{T_c^2(d_2 - d_1)N_0}{4A^2 T}, \end{aligned} \tag{62}$$

where $(\cdot)_S$ denotes the strobe correlator.

From (58) and (61), it is found that the CPEE because of the noise $n(\tau)$ has zero mean for narrow, wide, and strobe correlators. From (62), it is observed that the strobe correlator has the same CPEE variance because of the noise to the narrow correlator when $d_N = d_2 - d_1$. As a result, σ_1^2 in (57) is found as

$$\sigma_1^2 = \begin{cases} \sigma^2_{\delta\tau}(d_N) + \sigma^2_{1,N} & \text{for the narrow correlator} \\ \beta\sigma^2_{\delta\tau}(d_N) + \sigma^2_{1,W} & \text{for the wide correlator} \\ \sigma^2_{\delta\tau}(d_N) + \sigma^2_{1,S} & \text{for the strobe correlator,} \end{cases} \tag{63}$$

where $\sigma^2_{1,N}$, $\sigma^2_{1,W}$, $\sigma^2_{1,S}$, and $\sigma^2_{\delta\tau}$ are defined in (28), (29), (32), and (59), respectively, and $d_N = d_2 - d_1$ is assumed.

B. Rayleigh Channel

As found in (4), the overall CPEE from the resolved first arrival path in a Rayleigh channel is the sum of mutually independent errors such as the ED of the first arrival path, MI error, and noise. Then, the overall CPEE distribution becomes

$$f_{\tau,2}(\tau) = f_{\tau_{(1)}|(M,\tau_o)}(\tau) * f_{MI_2}(\tau) * f_{n,2}(\tau), \tag{64}$$

where $f_{\tau_{(1)}|(M,\tau_o)}(\tau)$ is defined in (49); $f_{MI_2}(\tau)$ is in (46), (47), or (48); and $f_{n,2}(\tau)$ represents the CPEE distribution because of the ACF output noise $n(\tau)$. Because the variance of the CPEE as a result of the noise $n(\tau)$ increases as the signal-to-noise ratio (SNR) decreases [4], $f_{n,2}(\tau)$ is wider in Rayleigh channels than in Rician channels. Let η be the ratio of the CPEE because of the noise in Rayleigh channel to the CPEE in Rician channel. Then, $f_{n,2}(\tau)$ can be expressed using a zero-mean normal

distribution with variance $\eta^2\sigma_{\delta\tau}^2$ and $\eta^2\sigma_{\delta\tau_S}^2$. Therefore,

$$f_{\tau,2}(\tau)\simeq\begin{cases} f_\tau^{\mathcal{N}}\left(\tau;0,\sigma_{2,N}^2+\eta^2\sigma_{\delta\tau}^2(d)\right)*f_{\tau_{(1)}|(M,\tau_o)}(\tau), \\ \qquad\text{for the narrow correlator}: d=d_N \\ f_\tau^{\mathcal{N}}(\tau;0,\sigma_{2,W}^2+\beta\eta^2\sigma_{\delta\tau}^2(d))*f_{\tau_{(1)}|(M,\tau_o)}(\tau), \\ \qquad\text{for the wide correlator}: d=d_W \\ f_\tau^{\mathcal{N}}(\tau;0,\sigma_{2,S}^2+\eta^2\sigma_{\delta\tau}^2(d))*f_{\tau_{(1)}|(M,\tau_o)}(\tau), \\ \qquad\text{for the strobe correlator}: d=d_2-d_1, \end{cases} \tag{65}$$

where $\sigma_{2,N}$, $\sigma_{2,W}$, $\sigma_{2,S}$, and $\sigma_{\delta\tau}^2$ are defined in (43), (44), (45), and (59), respectively, and $d_N = d_W/\beta = d_2 - d_1$. The positive mean of the CPEE occurs because of the ED of the detected first arrival path $\tau_{(1)}$.

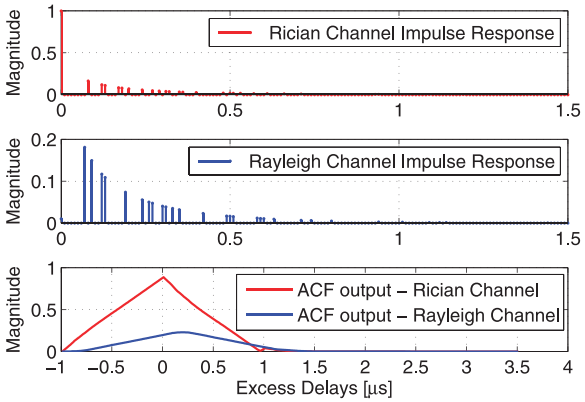

Fig. 6. ACF outputs in Rician and Rayleigh channels.

VI. SIMULATIONS FOR VERIFICATION

In practice, measuring an exact CPEE in the presence of the NLOS first arrival path, MI, and noise for various code phase discriminators and developing an empirical CPEE distribution model for various multipath environments are difficult tasks. Instead, we can use an empirical LMSC model to verify the theoretical analysis and mathematical models $f_{\tau,1}(\tau)$ (57) and $f_{\tau,2}(\tau)$ (65). ITU-R recommendation P.681-7 [11] generates LMSC impulse response $h_L(\tau)$, whose properties match those from the field observation in [14], and the ESDM-based ED PDF $f_\tau(\tau)$ (16) and PDS $f_P(\tau)$ (14) can be used to realize the statistical multipath channel impulse response $h_S(\tau)$ for a given number of individual multipath channels M. In this section, we compare the mathematical models of the CPEE distributions $f_{\tau,1}(\tau)$ (57) and $f_{\tau,2}(\tau)$ (65) and the ESDM-based CPEE distributions to the LMSC-based CPEE distributions.

To generate channel impulse responses for urban environments with the empirical model, we use the urban vehicular environment parameter values for the ITU-R recommendation P.681-7 LMSC model in [20] and [21]. The LMSC model generates a time-varying channel impulse response $h(\tau) = h_L(\tau)$ with $25 \le M \le 30$ for every 10 ms. When the LOS path of $h_L(\tau)$ is stronger than -5 dB (0 dB corresponds to about a 46 dB-Hz GNSS signal), the channel is considered a Rician channel, and when the LOS path is weaker than -15 dB, the channel is considered a Rayleigh channel. For each realization of $h_L(\tau)$, narrow, wide, and strobe correlators are applied to the noise-free ACF output

$$\begin{aligned} g_o(\tau) &= h(\tau)*R(\tau) \\ &= \left[\sum_{m=1}^{M} a_m e^{-j\theta_m}\delta(\tau-\tau_{(m)})\right]*R(\tau), \end{aligned} \tag{66}$$

and CPEEs are measured and collected to develop CPEE distributions (i.e., LMSC-based CPEE distributions) in noiseless Rician and Rayleigh channels. In addition, we generate the ESDM-based statistical channel impulse response $h(\tau) = h_S(\tau)$ for $M = 25$ independently realized mulipath channels with delay, and amplitudes follow the ED PDF $f_\tau(\tau)$ and ED PDS $f_P(\tau)$ to find the ESDM-based CPEE distributions for narrow, wide, and strobe correlators in noiseless Rician and Rayleigh channels. The $f_P(\tau)$ (14) has an exponentially decreasing density distribution, while any multipath in the LMSC model has at least about -15 dB less signal power. In addition, in Rician channel realizations using $f_\tau(\tau)$ and $f_P(\tau)$, the LOS path is given 0-dB signal power, and the second arrival NLOS path can have at most -5-dB signal power. In Rayleigh channel realizations, the first arrival path has at most -5-dB signal power. Fig. 6 shows examples of $h_S(t)$ and $|g_o(\tau)|$ $(=|h_S(\tau)*R(\tau)|)$ in Rician and Rayleigh channels. As shown, because of the short-delay paths, the ACF output loses its symmetry around the peak, and the ACF peak may appear at a delayed code phase in Rayleigh channels.

Figs. 7(a) and 7(b) show the CPEE distributions obtained from 10^5 Monte Carlo realizations of the LMSC model and the ESDM-based statistical channel model to test the mathematical models of the CPEE distributions $f_{\tau,1}(\tau)$ (57) and $f_{\tau,2}(\tau)$ (65). The legend shows the mean and standard deviation of the CPEE; for example, wide LMSC $[\mu, \sigma]$ and wide ESDM $[\mu, \sigma]$ represent the mean and the standard deviation of the LMSC-based CPEE distribution and the ESDM-based CPEE distribution for the wide correlator, respectively. As shown in Fig. 7(a), the ESDM-based CPEE distributions agree with the LMSC-based CPEE distributions. However, results for the wide correlator show a slight mismatch because the statistical channel model has an exponentially decreasing ED PDS $f_P(\tau)$, while the multipath amplitude of the LMSC model has a large step down from the LOS path, which results in a wider distribution of the ESDM-based CPEE shown in Figs. 7(a) and 7(b). Overall, there is good agreement between the ESDM-based CPEE distributions and the LMSC-based CPEE distributions. First, the CPEE distribution for the wide correlator is wider than those for the narrow and strobe correlators, which agrees with that $\sigma_{1,W}$ (29) $> \sigma_{1,N}$ (28). Second, the CPEE distributions for the wide, narrow, and strobe correlators have a negligibly small mean comparing to their standard deviation. The

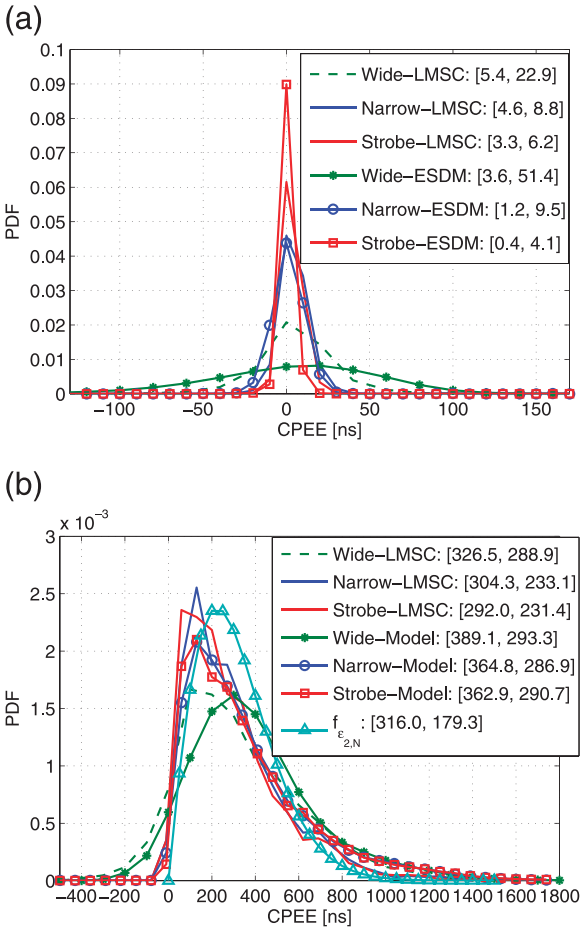

Fig. 7. Comparison of CPEE distributions in noiseless channel.

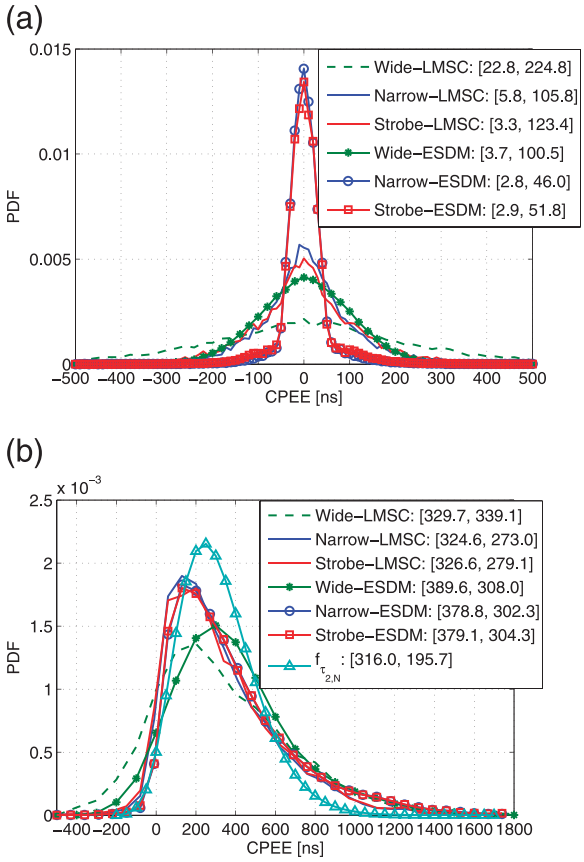

Fig. 8. Comparison of CPEE distributions in noisy channel.

second observation agrees with the mathematical analysis for $f_{MI_{1,N}}(\tau)$ (30), $f_{MI_{1,W}}(\tau)$ (31), and $f_{MI_{1,S}}(\tau)$ (32).

Figs. 8(a) and 8(b) show the comparison of the CPEE distributions for wide, narrow, and strobe correlators in noisy Rician and Rayleigh channels. The resulting ACF output is corrupted by $n_c(\tau)$ as

$$g_n(\tau) = h(\tau) * R(\tau) + n_c(\tau), \tag{67}$$

where $n_c(\tau)$ is a colored noise with covariance

$$E[n_c(\tau)n_c^*(\tau-\Delta)] = \begin{cases} N_t(1-|\Delta|/T_c), & |\Delta| \le T_c \\ 0, & \text{otherwise}, \end{cases} \tag{68}$$

and $N_t = Nf_sT_cN_0$, sampling rate f_s, and coherent correlation length NT_c [4]. In the simulations, N_t is set to obtain a fixed target SNR (15 dB) at the ACF output, which is assumed because GNSS receivers try to integrate sufficiently long to have a good SNR at the ACF output in practice. As expected from (63), the CPEE distribution in noisy Rician channels follows normal distribution, as shown in Fig. 8(a).

Comparing Figs. 7(a) and 8(a), the LMSC-based CPEE distributions become wider than the ESDM-based CPEE distributions for the addition of noise, which concludes that the effect of noise is smaller with the ESDM-based statistical channel model than with the empirical LMSC model. This is because very short-delay paths have stronger power (because of the exponentially decreasing ED PDS $f_P(\tau)$) in the statistical channel than in the LMSC. Thus, the very short-delay paths often contribute to build a strong resolved first arrival path, which results in a smaller CPEE variance in the ESDM-based CPEE distributions. The CPEE distributions in Figs. 7(a) and 8(a) are similar to the Gaussian distribution, which verifies the validity of the mathematical models in (33)–(35) and (51)–(53).

However, in noisy Rayleigh channel simulations shown in Fig. 8(b), the CPEE distributions for narrow, strobe, and wide correlators have shapes similar to those in the noiseless Rayleigh channel. The effect of $f_{n,2}(\tau)$ on the CPEE is not very noticeable, and $f_{\varepsilon_2}(\tau)$ in (51), (52), or (53) governs $f_{\tau,2}(\tau)$ (64). However, when the SNR is low, it is expected that the effect of $f_{n,2}(\tau)$ on the CPEE distribution increases so that $f_{\tau,2}(\tau)$ can look different from $f_{\varepsilon_2}(\tau)$. In Figs. 7(b) and 8(b), the ESDM-based CPEE distribution for the wide correlator has a slightly larger positive mean ED and wider distribution than the LMSC-based CPEE distribution. These results are again because of the difference between the ESDM-based statistical channel model and the empirical LMSC model. Overall, the results in Figs. 7 and 8 obtained from the empirical LMSC model and the ESDM-based statistical channel model show a good match with the mathematical CPEE distribution model f_{ε_2} and f_{τ_2}.

VII. CONCLUSION

In this paper, the effects of the ED of the first arrival path, MI, and noise on the CPEE for narrow, wide, and strobe correlators in Rician and Rayleigh channels have been theoretically analyzed, and mathematical models of the CPEE distributions have been developed. In addition, based on 2D ESDM, the statistical ED PDF and PDS of the GNSS multipath have been derived, and the ESDM-based CPEE distributions of the resolved first arrival path for wide, narrow, and strobe correlators in Rician and Rayleigh channels have been obtained. The mathematical models of CPEE distribution have been compared to the ESDM-based CPEE distributions and the empirical LMSC-based CPEE distributions and have shown to be good matches in general. The mathematical models and theoretical analysis of the CPEEs from the resolved first arrival path are useful to develop insights into GNSS multipath errors and are essential for developments of algorithms against multipath distortion and measurement errors.

REFERENCES

[1] Agarwal, N., Basch, J., Beckmann, P., Bharti, P., Bloebaum, S., Casadei, S., Chou, A., Enge, P., Fong, W., Hathi, N., Mann, W., Sahai, A., Stone, J., Tsitsiklis, J., and Roy, B. V.
Algorithms for GNSS operation indoors and downtown.
GNSS Solutions, **6**, 3 (Dec. 2002), 149–160.

[2] Steingass, A., and Lehner, A.
Measuring the navigation multipath channel: A statistical Analysis.
In *Proceedings of the 17th International Technical Meeting of the Satellite Division of the Institute of Navigation (GNSS)*, Long Beach, CA, Sept. 2004, 1157–1164.

[3] Kong, S. H.
Statistical analysis of urban GPS multipath and pseudo-range measurement errors.
IEEE Transactions on Aerospace and Electronic Systems, **47**, 2 (Apr. 2011), 1101–1113.

[4] Misra, P., and Enge, P.
Global Positioning System: Signals, Measurements, and Performance, 2nd ed. Massachusetts: Ganga-Jamuna Press, 2006.

[5] Braasch, M. S.
Multipath effects. In
Global Positioning System: Theory and Applications, Vol. 1, Parkinson, B., and Spilker, J. Eds. Washington, DC: American Institute of Aeronautics and Astronautics, 1996, 547–568.

[6] Van Dierendonck, A. J., Fenton, P., and Ford, T.
Theory and performance of narrow correlator spacing in a GPS receiver.
Navigation, **39**, 3 (Fall 1992), 265–284.

[7] Janaswamy, R.
Angle and time of arrival statistics for the Gaussian scatter density model.
IEEE Transactions on Wireless Communications, **1**, 3 (July 2002), 488–497.

[8] Kong, S. H.
TOA and AOD statistics for down link Gaussian scatterer distribution model.
IEEE Transactions on Wireless Communications, **8**, 5 (May 2009), 2609–2617.

[9] Turin, G. L., Clapp, F. D., Johnston, T. L., Fine, S. B., and Lavry, D.
A statistical model of urban multipath propagation.
IEEE Transactions on Vehicular Technology, **21**, 1 (Feb. 1972), 1–9.

[10] Ur Rehman, M., Chen, X., Parini, C. G., and Ying, Z.
Evaluation of a statistical model for the characterization of multipath affecting mobile terminal GPS antennas in sub-urban areas.
IEEE Transactions on Antennas and Propagation, **60**, 2 (Feb. 2012), 1084–1094.

[11] Propagation Data Required for the Design of Earth–Space Land Mobile Telecommunication Systems. International Telecommunications Union Recommendations Section. Recommendation P.681-7, Oct. 2009.

[12] Irsigler, M., and Eissfeller, B.
Comparison of multipath mitigation techniques with consideration of future signal structures.
In *Proceedings of the 16th International Technical Meeting of the Satellite Division of the Institute of Navigation (GPS/GNSS)*, Portland, OR, Sept. 2003, 2584–2592.

[13] Papoulis, A.
Probability, Random Variables and Stochastic Processes, 3rd ed. New York: McGraw-Hill, 1991.

[14] Lehner, A., and Steingass, A.
A novel channel model for land mobile satellite navigation.
In *Proceedings of the 18th International Technical Meeting of the Satellite Division of the Institute of Navigation (GNSS)*, Long Beach, CA, Sept. 2005, 2132–2138.

[15] Liberty, J. C., Jr., and Rappaport, T. S.
Smart Antennas for Wireless Communications: IS-95 and Third Generation CDMA Applications. New Jersey: Prentice Hall PTR, 1999.

[16] Jakes, W. C.
Microwave Mobile Communication. New York: IEEE Press, 1974.

[17] Ertel, R. B., and Reed, J. H.
Angle and time of arrival statistics for circular and elliptical scattering models.
IEEE Journal on Selected Areas in Communications, **17** (Nov. 1999), 1829–1840.

[18] Kalkan, M.
A statistical model of mobile signal reception. *Proceedings of the 3rd International Conference on Universal Personal Communications*, San Diego, CA, 1994, 150–154.

[19] Goldsmith, A.
Wireless Communications. New York: Cambridge University Press, 2005.

[20] Krach, B., Steingass, A., and Lehner, A.
Technical note on the implementation of the land mobile satellite channel model-software usage. German Aerospace Center DLR, DLR-KN-FS-02-07, 2, DLR (June 2007).

[21] Nam, W., and Kong, S. H.
Least-squares–based iterative multipath super-resolution technique.
IEEE Transactions on Signal Processing, **61**, 3 (Feb. 2013), 519–529.

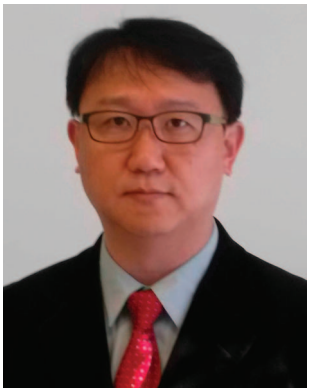

Seung-Hyun Kong (M'06) received a B.S.E.E. degree from the Sogang University, Korea, in 1992; an M.S.E.E. degree from the Polytechnic University, New York, in 1994; and a Ph.D. degree in aeronautics and astronautics from Stanford University, California, in 2006. From 1997 to 2004, he was with Samsung Electronics and Nexpilot, both in Korea, where his research focus was on 2G CDMA and 3G UMTS PHY and mobile positioning technologies. In 2006, he was involved with hybrid positioning technology development using wireless location signature and assisted GNSS at Polaris Wireless, and from 2007 to 2009, he was a research staff member at Qualcomm Research Center, San Diego, California, where his research and development focus was on indoor location technologies and advanced GNSS technologies. Since 2010, he has been an assistant professor at the Department of Aerospace Engineering in the Korea Advanced Institute of Science and Technology. His research interests include superresolution signal processing, detection and estimation for navigation systems, and assisted GNSS in wireless communication systems.